

## Effect of Heat Treatment on Pore Architecture and Associated Property Changes in Plasma Sprayed TBCs

**S. Paul, I. O. Golosnoy, A. Cipitria, T. W. Clyne**

*Department of Materials Science & Metallurgy, University of Cambridge, Cambridge, UK*

**L. Xie, M. R. Dorfman**

*Sulzer Metco (US) Inc., Westbury, New York, USA*

### Abstract

Plasma sprayed Thermal Barrier Coatings (TBCs) exhibit many interlamellar pores, voids and microcracks. These microstructural features are primarily responsible for the low global stiffnesses and the low thermal conductivities commonly exhibited by such coatings. The pore architecture thus has an important influence on such thermophysical properties. In the present work, the effect of heat treatment (at temperatures up to 1400°C, for times of up to 10 hours) on the pore architecture in detached YSZ top coats has been characterised by Mercury Intrusion Porosimetry (MIP) and gas-sorption techniques. While the overall porosity level remained relatively unaffected (at around 10-12%) after the heat treatments concerned, there were substantial changes in the pore size distribution and the (inter-connected) specific surface area. Fine pores (<~50 nm) rapidly disappeared, while the specific surface area dropped dramatically, particularly at high treatment temperatures (~1400°C). These changes are thought to be associated with intra-splat microcrack healing, improved inter-splat bonding and increased contact area, leading to disappearance of much of the fine porosity. These microstructural changes are reflected in sharply increased stiffness and thermal conductivity. Measured thermal conductivity data are compared with predictions from a recently-developed analytical model [1], using the deduced inter-splat contact area results as input parameters. Good agreement is obtained, suggesting that the model captures the main geometrical effects and the pore size distribution measurements reflect the most significant microstructural changes.

### Introduction

Ceramic Thermal Barrier Coatings (TBCs) are being increasingly used to protect metallic components of gas turbines exposed to elevated temperatures. Typical TBC systems are composed of a YSZ top coat about 100-500 µm in thickness,

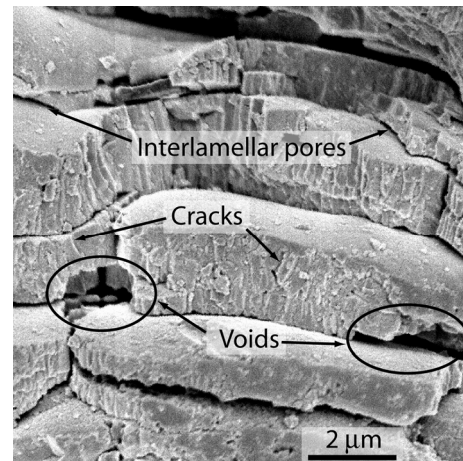


*Figure 1: Typical microstructural features of as-sprayed TBC top coat.*

deposited either by atmospheric plasma spray (APS) or electron beam physical vapour deposition (EB-PVD) onto a metallic bond coat. Plasma-sprayed deposits are composed of splats created by quenching of molten or sometimes semi-molten feedstock particles either on a bare substrate or on a layer of previously deposited particles. This rapid cooling of the splats results in the formation of large number of microcracks. The through-thickness microcracks relax a lot of the quenching stress generated during plasma spraying [2].

Common features of the microstructure of APS coatings are shown in Fig. 1. Presence of such microstructural features give rise to its low macroscopic stiffness and thermal conductivity. Thus, properties of these coatings depend not only on the overall porosity, but also on the orientation, size and shape of the pores. While estimation of the overall porosity is fairly straightforward, understanding and quantifying its distribution is difficult. Several techniques have been applied to determine pore architecture in thermal spray deposits: image analysis,

Mercury Intrusion Porosimetry (MIP), gas adsorption and Small Angle Neutron Scattering (SANS). Each technique has its advantages and limitations.

Image analysis is probably the least time consuming of the above mentioned methods, but it lacks accuracy, usually neglects the fine scale porosity and is often user dependent. These disadvantages are overcome by gas adsorption technique, which captures the fine scale porosity and gives an estimate of pore-size distribution based on assumed pore geometry. However, this technique is time consuming and no information is obtained regarding the large global pores. SANS on the other hand is a radiation scattering technique which is most effective for the study of orientation of pores below 500 nm. The equipment is very expensive and use of this technique for routine analysis is not realistic. MIP gives measure of both overall porosity and pore-size distribution. It measures both globular pores and fine scale porosity based on a given geometry. State-of-the-art MIP equipment can measure pores from 4 nm to about 300  $\mu\text{m}$ . However, the technique is time consuming and uses mercury which sometimes causes concern with safe disposal. An overview of different methods for pore size characterisation and their application range can be found elsewhere [3].

In the present work, effect of change in pore size distribution on thermo-physical properties is evaluated and an explanation is also provided on observed changes in stiffness and thermal conductivity.

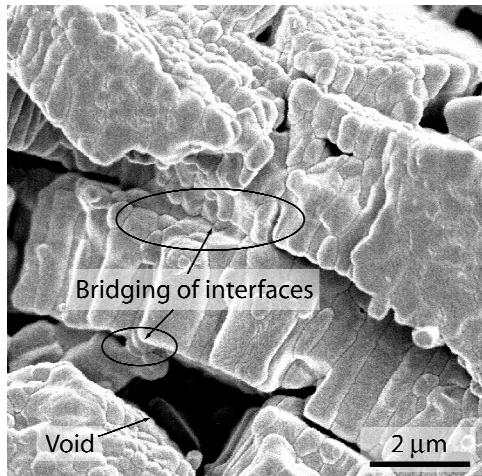


Figure 2: Micrograph of a top coat heat treated at 1400°C for 10 h.

## Experimental

### Sample Preparation

**Coating production:** YPSZ ( $\text{ZrO}_2$ -7.6 wt.%  $\text{Y}_2\text{O}_3$ ) powder, designated 204NS, supplied by Sulzer Metco (Westbury, NY, USA), was air plasma sprayed onto 1.5 mm thick mild steel substrates. The top coat was de-bonded from the substrate by

treating it with hydrochloric acid. YSZ top coat with varying thickness (0.8-2.5 mm) were produced using the conditions shown in Table 1.

Table 1: Plasma spraying parameters.

Chamber pressure	Atmospheric
Stand-off distance, mm	105
Arc current, A	750
Voltage, V	60
Gun speed, $\text{mm s}^{-1}$	55
Gun type	F4
Nozzle internal diameter, mm	8
Ar flow rate, lpm	50
$\text{H}_2$ flow rate, lpm	8
Scanning step (mm)	8

**Heat treatment:** The detached top coats were isothermally heat treated in air at 1200°C and 1400°C for different times. A heating rate of  $\sim 20^\circ\text{C}/\text{min}$  was used, followed by air cooling after heat treatment to avoid formation of any monoclinic phase [4]. This was also confirmed by x-ray diffraction studies.

### Dimensional, Stiffness and Thermal Conductivity Changes

**Dilatometry:** Dimensional change during isothermal heat treatment was monitored using DIL 402C dilatometer (Netzsch, Selb, Germany). Dilatometry was performed on detached top coats, in both in-plane and through-thickness directions.

**Stiffness measurement:** Stiffness measurements were made using a purpose-built four-point bending rig. Load was applied via a counter-balanced plattform, using small pre-weighed masses and displacements were measured using a scanning laser extensometer. The elastic behaviour was confirmed by checking the linearity and reversibility of the load-deflection plots.

**Thermal conductivity measurement:** Thermal conductivity of the detached top coats was measured using both HotDisk<sup>®</sup> method [5] and a simple steady-state bi-substrate technique. The bi-substrate technique is based on establishing a steady-state heat flow through the sample, sandwiched between a pair of metallic blocks with known thermal properties. Full details of the setup can be found elsewhere [6].

### Porosity and Microstructure

**Scanning electron microscopy:** JEOL 6340F FEG-SEM was used to study the coating microstructure. As-sprayed coatings exhibit the characteristic layered structure of PS coatings. The structure within the splat shows columnar grains (Fig. 2). Microcracks and inter-splat porosity, as shown in Fig. 1, mostly have slit type geometry. Heat treatment results in grain growth, often bridging interfaces between splats in close physical proximity, as shown in Fig. 2. There is also evidence of the healing of microcracks. However, large voids remain relatively unaffected.

**Mercury Intrusion Porosimetry (MIP):** A Micro Meritics AutoPore IV (one micromeritics drive, Norcross, GA 30093-1877, USA) was used to estimate the pore-size distribution and the total volume of surface-connected porosity. Known mass of the sample was placed in a glass penetrometer, which was evacuated and then back-filled with mercury. Since mercury behaves as a non-wetting liquid for most oxide systems, it needs to be forced into the specimen by application of external pressure. The pressure required being inversely proportional to the pore width, in accordance with the Washburn equation [7] for slit-like pores:

$$P = -\frac{2\gamma \cos \theta}{d_v} \quad (1)$$

Where  $P$  is the applied pressure,  $\gamma$  is the surface tension of mercury (taken as  $0.485 \text{ N m}^{-1}$ ),  $\theta$  is the contact angle (taken as  $130^\circ$ ) and  $d_v$  is the slit width. The penetrometer was progressively pressurized up to  $\sim 200 \text{ MPa}$ , with the penetration volume being monitored by measuring the capacitance of a coaxial capacitor formed by the intruding mercury and the conducting stem. Pore size distribution was thus obtained, as well as the pore volume. Estimates of sample skeletal and bulk densities were also deduced from the pore volume measurements.

**Gas adsorption:** A MicroMeritics TriStar 3000 (one micromeritics drive, Norcross, GA 30093-1877, USA) was used to measure the specific surface area and fine scale porosity of detached top coats. Samples were dried thoroughly ( $\sim 250^\circ\text{C}$  overnight) before measurement. The sample chambers were then cooled to liquid  $\text{N}_2$  temperature and evacuated. Nitrogen was then introduced in controlled pressure increments, and the equilibrated pressures measured and compared with the saturation pressure, to determine the quantities of adsorbed gas. The Brunauer–Emerett–Teller (BET) adsorption isotherm was then used to determine the specimen surface area.

### Porosity and Pore Architecture

#### Specific Surface Area

The surface area of the coatings reduced drastically from  $\sim 0.3 \text{ m}^2 \text{ g}^{-1}$  for as-sprayed coatings to  $\sim 0.1 \text{ m}^2 \text{ g}^{-1}$  after heat treatment at  $1400^\circ\text{C}$  for 1 h. This reduced further to  $\sim 0.07 \text{ m}^2 \text{ g}^{-1}$  when the samples were heat treated for 10 h. This reduction in surface area can be explained in the light of disappearance of small pores by sintering after heat treatment (Fig. 3). These small pores do not contribute much to porosity, but contribute significantly to the overall surface area.

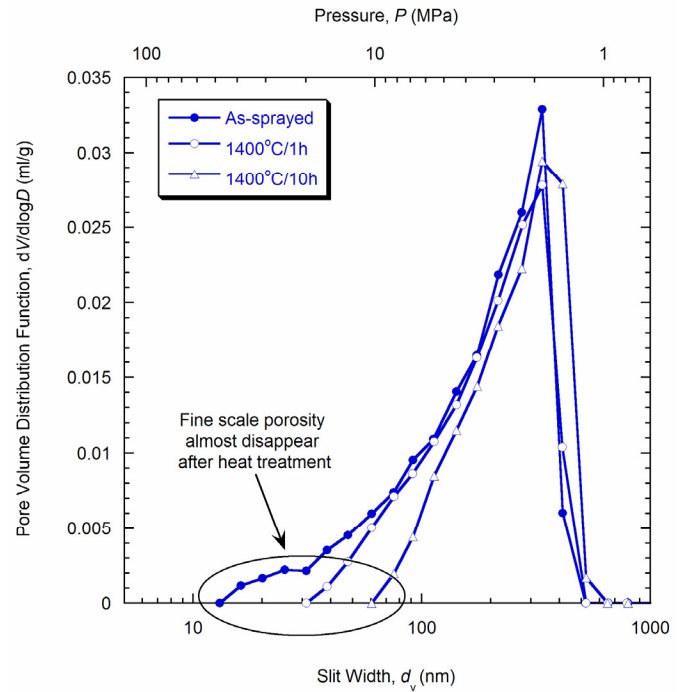


Figure 3: Pore size distribution of top coat in both as-sprayed condition and after isothermal heat treatment at  $1400^\circ\text{C}$ .

#### Pore Size Distribution

The pore size distribution obtained from MIP is shown in Fig. 3. Only the distribution up to  $\sim 1 \mu\text{m}$  is shown as no change in the distribution of larger pores was observed. By using Eq. (1), estimate can be made of the overall porosity level, and of the pore size distribution. It can be seen from Fig. 3 that the pores size distribution is sensitive to the conditions to which the coating is subjected to prior to testing. The disappearance of fine scale porosity, would affect various properties of the coating, particularly stiffness.

The pore size distribution has been obtained assuming slit-like pore geometry. While this assumption does not affect the deduced pore volume or overall porosity, but this would affect the pore size distribution [8]. Another concern regarding analysis of mercury porosimetry data is the presence of “ink-bottle” or “hour-glass” shaped pores [9]. Whenever pores increase in size, beyond a constriction, called the throat, the deduced distribution will be skewed towards finer pores. However, it has been demonstrated that this is not a great problem for widely interconnected network of pores [10].

Finally, from the deduced pore size distribution and assuming reversible work of intrusion [11], the specific surface area can be obtained from MIP data using Eq. (2):

$$S = -\frac{1}{\gamma \cos \theta} \int_0^V P dV \quad (2)$$

Where  $S$  is the specific surface area and  $V$  is the volume of mercury intruded at highest applied pressure. Applying this equation, a value  $S \sim 0.26 \text{ m}^2 \text{ g}^{-1}$  was obtained for as-sprayed sample. The value of  $S$  reduces to  $\sim 0.16 \text{ m}^2 \text{ g}^{-1}$  and  $\sim 0.11 \text{ m}^2 \text{ g}^{-1}$  for samples heat treated at  $1400^\circ\text{C}$  for 1 h and 10h respectively. These values of  $S$  are slightly larger than that obtained from BET measurements. Such discrepancies are common [12], and are often due, at least in part, to the ink-bottle type pores, which skew the distribution towards finer pores, raising the surface area. Another factor that might also contribute to the discrepancy is that the deduction of surface area in Eq. (2) is based on the assumption that movement of mercury meniscus in the sample is reversible. As this is rarely the case for interconnected pore network, Eq. (2) is not strictly valid for porous samples which contain such interconnected pores.

### Effect of Pore Architecture on Coating Properties

#### Stiffness

The Young's modulus of as-sprayed top coat was found to be  $\sim 22 \text{ GPa}$ . This is in good general agreement with the data available in literature taking into account the variation one can have due to different spraying conditions [13, 14]. This value is an order of magnitude lower than the corresponding bulk material. This reduction is attributed to the presence of defects, particularly the fine scale porosity mostly in the form of microcracks. Poor bonding between splats can also lead to sliding of the splats past each other, thus leading to a low macroscopic stiffness. These defects results in high compliance of the as-sprayed coating, allowing it to accommodate thermal and mechanical strains induced during service.

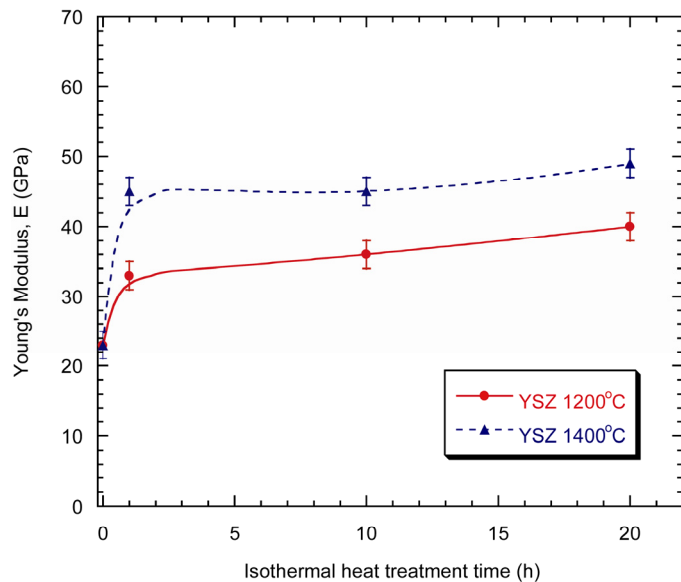


Figure 4: Young's modulus data of detached top coat subjected to prior heat treatments.

While in service, the stiffness of the top coat changes and this has been presented in Fig. 4. It can be seen that substantial increase in stiffness can arise, particularly after heat treatment at  $1400^\circ\text{C}$ . The stiffness shows an initial sharp rise followed by a more progressive rise [15]. MIP studies of both as-sprayed and heat-treated top coats show that there is a considerable decrease in the volume of fine scale porosity. The pores smaller than  $\sim 50 \text{ nm}$  seem to almost disappear after heat treatment (Fig. 3). This reduction in fine scale porosity, in the form of healing of microcracks is responsible for the sharp increase in the stiffness of these coatings.

#### Shrinkage

Dilatometry data, where the linear contraction is plotted against time at temperature are presented in Fig. 5. Shrinkage occurs due to sintering of the fine scale features in the top coat (TC). For a given direction, the shrinkage is faster at  $1400^\circ\text{C}$ , and in all cases the rate of contraction falls off with time. It is also clear that contraction is anisotropic, with more shrinkage taking place in the through-thickness direction as compared to the in-plane direction. This effect has been reported previously for PS zirconia [16].

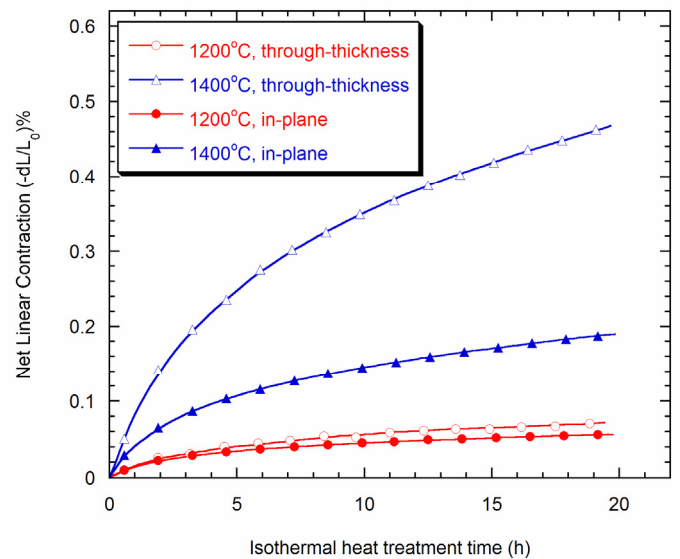


Figure 5: Dilatometry plots obtained during isothermal heat treatment of top coats.

It must be noted that in-plane shrinkage is probably more important from the point of view of thermal stress generation. Thus a lower value of in-plane shrinkage would lead to longer life of the coating.

Considering no thermal mismatch strain and using Eq. (3), biaxial stress values of  $\sim 30 \text{ MPa}$  and  $\sim 120 \text{ MPa}$  were estimated for the coating heat treated at  $1200^\circ\text{C}$  and  $1400^\circ\text{C}$  for 20 h. However, it must be noted that at elevated temperatures various stress relaxation mechanisms operate, relieving a lot of this stress.

$$\sigma = \frac{\varepsilon E}{(1-\nu)} \quad (3)$$

Where  $\varepsilon$  is the strain induced due to shrinkage,  $E$  is the Young's modulus of the coating (taken from Fig. 4),  $\nu$  is the Poisson ratio (taken as 0.2) and  $\sigma$  is the bi-axial stress.

### Thermal Conductivity

*A simple analytical model:* A simple analytical model based on geometrical representation of the microstructure of plasma sprayed coatings has been used to predict its thermal conductivity. Full details of the model can be found elsewhere [1].

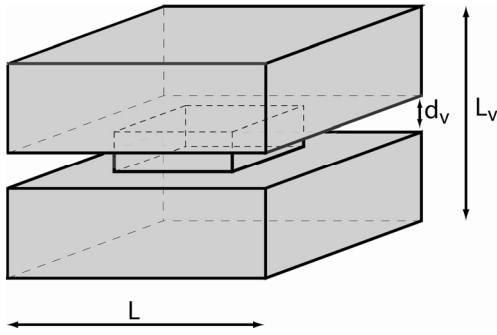


Figure 6: Schematic representation of the unit cell used for model prediction.

The microstructure of the top coat has been modeled as a periodic array of lamellae, separated by pores, with contact bridges between them (figure 6). In the analytical model, the top coat is divided into two regimes, within which the heat flow occurs either by unidirectional serial flow through the splats and pores or by being funneled through the regions of the splat above and below the bridges. After heat treatment, the pore architecture changes and contact bridge area also increases (Fig. 7). This leads to an increase in the thermal conductivity.

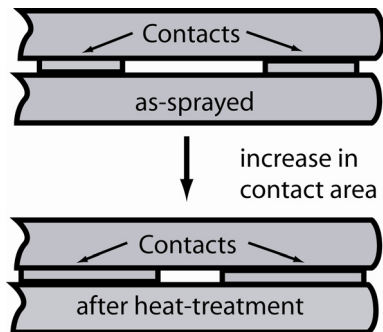


Figure 7: Schematic representation of the change in microstructure due to heat treatment.

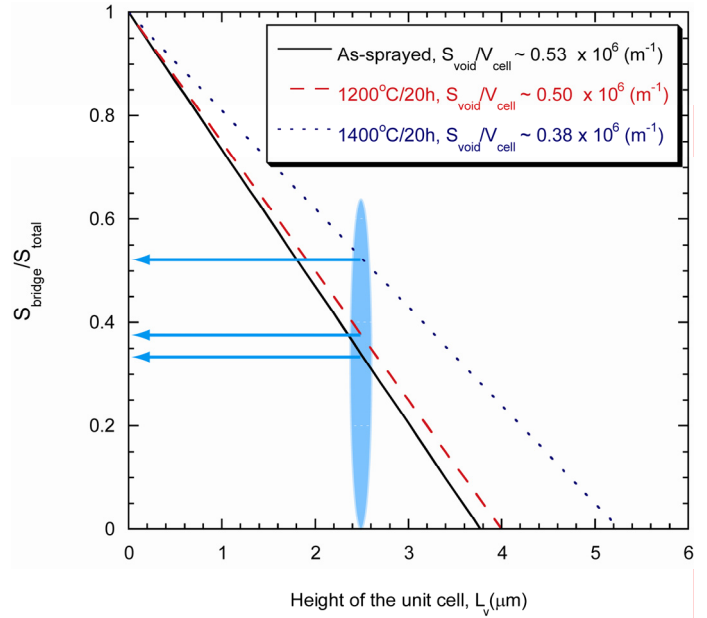


Figure 8: Normalised bridge area as a function of heat treatment and modeled splat thickness.

Input parameters for the model, such as thickness of splat ( $L_v$ ), width of the pore ( $d_v$ ), were obtained from SEM, single splat experiment and MIP. Different surface to volume ratios ( $S_{\text{void}}/V_{\text{cell}}$ ) were obtained for as-sprayed and heat-treated samples from MIP. Eq. 2 was employed to obtain the  $S_{\text{void}}$  for a given pore size range, while  $V_{\text{cell}}$  was directly obtained from the mercury intrusion volume. The normalized bridge area ( $S_{\text{bridge}}/S_{\text{total}}$ ), obtained by incorporating the MIP data into the geometrical model changes from  $\sim 0.34$  for as-sprayed sample to  $\sim 0.38$  and  $\sim 0.53$  for sample heat treated at  $1200^\circ\text{C}/20\text{ h}$  and  $1400^\circ\text{C}/20\text{ h}$  respectively (Fig. 8). These values of the increased bridge area would increase the area through which heat conduction takes place in the coating, thereby increasing its effective thermal conductivity.

The predicted thermal conductivity increases from  $\sim 0.9\text{ W m}^{-1}\text{ K}^{-1}$  for as-sprayed sample to  $\sim 1.6\text{ W m}^{-1}\text{ K}^{-1}$  for sample heat-treated at  $1400^\circ\text{C}/20\text{ h}$ . However, for samples heat treated at  $1200^\circ\text{C}/20\text{ h}$  very slight increase in thermal conductivity was observed. Good agreement can be seen between the predicted and observed thermal conductivity values in Fig. 9. It is interesting to note that heat treatment at  $1200^\circ\text{C}/20\text{ h}$  brings about two fold increase in stiffness, while the thermal conductivity is not significantly altered. Thus, one may conclude that while heat treatment at lower temperature might cause healing of microcracks, high temperature heat treatment causes enhanced sintering necessary to cause notable increase in the bridge area to bring about drastic change in the thermal conductivity of the top coat.

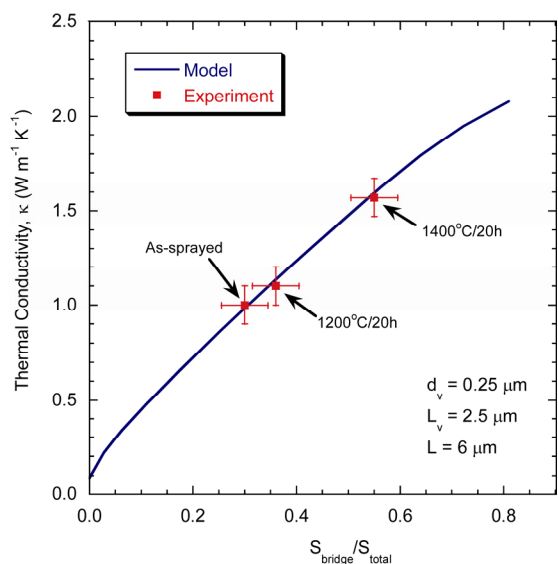


Figure 9: Comparison between experimental and predicted thermal conductivity values for as-sprayed and heat-treated top coats.

### Summary and Conclusion

Porosity and pore architecture governs some of the most important thermo-physical properties of plasma sprayed (PS) coatings. The presence of large number of defects, in the form of inter-lamellar pores and microcracks, are responsible for low microscopic stiffness of PS top coats (~22 GPa). The density of such defects reduces significantly after heat treatment, particularly fine scale porosity <~50 nm (pore width), which leads to a sharp rise in stiffness of the coating. The stiffness of the top coat rose to ~33 GPa and ~45 GPa after a heat treatment at 1200°C/20 h and 1400°C/20 h. Thermal conductivity also increased with heat treatment due to increase in the area of contact between the splats. Thermal conductivity increased from ~1 W m<sup>-1</sup> K<sup>-1</sup> for as-sprayed sample to ~1.2 W m<sup>-1</sup> K<sup>-1</sup> and ~1.6 W m<sup>-1</sup> K<sup>-1</sup> for samples heat treated at 1200°C/20 h and 1400°C/20 h. These experimental values agree well with the predicted thermal conductivity values.

### Acknowledgements

Financial support for this work has come from Sulzer Metco, the Gates Cambridge Trust and EPSRC, via a platform grant.

### References

1. I. O. Golosnoy, S.A. Tsipas, and T.W. Clyne, An Analytical Model for Simulation of Heat Flow in Plasma Sprayed Thermal Barrier Coatings, *J. Therm. Spray Technol.*, Vol 14 (No. 2), 2005, p. 205-214.
2. S. Kuroda and T.W. Clyne, The Quenching Stress in Thermally Sprayed Coatings, *Thin Solid Films.*, Vol 200, 1991, p. 49-66.

3. J. Rouquerol, D. Avnir, C. W. Fairbridge, D. H. Everett, J. H. Haynes, N. Pernicone, J. D. F. Ramsay, K. S. W. Sing, and K. K. Unger, Recommendations for the characterisation of porous solids, *Pure Appl. Chem*, Vol 66 (No. 8), 1994, p. 1739-1758.
4. J. Moon, H. Choi, H. Kim, and C. Lee., The effects of heat treatment on the phase transformation behaviour of plasma-sprayed stabilized ZrO<sub>2</sub> coatings, *Surf. Coat. Technol.*, Vol 155 (No. 1), 2002, p. 1-10.
5. S. E. Gustafsson, Transient Plane Source Techniques for Thermal Conductivity and Thermal Diffusivity Measurements of Solid Materials, *Rev. Sci. Inst.*, Vol 62 (No. 3), 1990, p. 797-804.
6. J. C. Tan, S. A. Tsipas, I. O. Golosnoy, J. A. Curran, S. Paul, and T. W. Clyne, A Steady-state Bi-substrate Technique for Measurement of the Thermal Conductivity of Ceramic Coatings. *Surf. Coat. Technol.*, 2006. Vol 201 (No. 3-4), 2006, p. 1414-1420.
7. E. W. Washburn, Note on a Method of Determining the Distribution of Pore Sizes in a Porous Materials, *Proc. Natl. Acad. Sci. USA.*, Vol 7, 1921, p. 115-116.
8. J. Ilavsky, C.C. Berndt, and J. Karthikeyan, Mercury intrusion porosimetry of plasma-sprayed ceramic, *J. Mater. Sci.*, Vol 32 (No. 15), 1997, p. 3925-3932.
9. L. Moscou and S. Lub, Practical Use of Mercury Porosimetry in the Study of Porous Solids, *Powder Technol.*, Vol 29, 1981, p. 45-52.
10. N. C. Wardlaw and M. McKellar, Mercury Porosimetry and the Interpretation of Pore Geometry in Sedimentary-Rocks and Artificial Models, *Powder Technol.*, Vol 29 (No. 1), 1981, p. 127-143.
11. H. M. Rootare and C.F. Prenzlow, Surface Areas from Mercury Porosimeter Measurements, *J. Phys. Chem.*, Vol 71 (No. 8), 1967, p. 2733-2736.
12. P. J. Dees and J. Polderman, Mercury porosimetry in pharmaceutical technology. *Powder Technol.*, Vol 29, 1981, p. 187-197.
13. D. Schwingel, R. Taylor, T. Haubold, J. Wirgenn, and C. Gaulco, Mechanical and Thermophysical properties of thick PYSZ Thermal Barrier Coatings: Correlation with Microstructure and Spraying Parameters, *Surf. Coat. Technol.*, Vol 108-109, 1998, p. 99-106.
14. J. S. Wallace and J. Ilavsky, Elastic Modulus Measurements in Plasma Sprayed Deposits, *J. Therm. Spray Technol.*, Vol 7 (No. 4), 1998, p. 521-526.
15. J. A. Thompson and T.W. Clyne, The Effect of Heat Treatment on the Stiffness of Zirconia Top Coats in Plasma-Sprayed TBCs, *Acta Mater.*, Vol 49 (No. 9), 2001, p. 1565-1575.
16. S. A. Tsipas, I. O. Golosnoy, R. Damani, and T. W. Clyne, The Effect of a High Thermal Gradient on Sintering and Stiffening in the Top Coat of a Thermal Barrier Coating (TBC) System, *J. Therm. Spray Technol.*, Vol 13 (No. 3), 2004, p. 370-376..